EUROPEAN JOURNAL OF BIOMEDICAL AND PHARMACEUTICAL SCIENCES
http://www.ejbps.com

ISSN 2349-8870
Volume: 3
Issue: 5
487-494
Year: 2016

EFFECT OF G67R AND G207E MUTATIONS ON STABILITY OF ARYLAMINE N-ACETYLTRANSFERASE IN ISONIAZID RESISTANCE STRAINS OF *MYCOBACTERIUM TUBERCULOSIS* REVEALED BY MOLECULAR DYNAMICS SIMULATION STUDY

Lingaraja Jena, Shraddha Deshmukh, Tapaswini Nayak, Gauri Wankhade, Bhaskar C. Harinath*

Bioinformatics Centre, JBTDRC, MGIMS, Sevagram, Maharashtra, India.

***Corresponding Author: Dr. Bhaskar C. Harinath**
Bioinformatics Centre, JBTDRC, MGIMS, Sevagram, Maharashtra, India.

Article Received on 09/03/2016 **Article Revised on 29/03/2016** **Article Accepted on 19/04/2016**

ABSTRACT
Isoniazid (INH) is a front line drug used in the treatment of tuberculosis (TB) that remains a major cause of death worldwide. Isoniazid is a prodrug, requiring activation in the mycobacterial cell by the catalase / peroxidase activity of the KatG whereas arylamine N-acetyltransferase (NAT), a drug-metabolizing enzyme of MTB (Rv3566c) can acetylates isoniazid by transferring an acetyl group from acetyl coenzyme A to the terminal nitrogen of INH. Two mutations in NAT enzymes (G67R and G207E) were reported in clinical isolates of MTB associated with INH resistance. To study the effect of these mutations on NAT, molecular dynamics (MD) simulation analysis was performed for both wild type and two mutant models of NAT. Additionally, we performed docking of INH with the foresaid models of NAT enzyme followed by MD simulation of respective protein-ligand complexes. We have found that the binding site pocket was more stable in NAT_G67R mutant and the residues of this mutant model fluctuate less in both bound and unbound cases. In mutant models, the alteration of Gly to Arg (G67R) or Glu (G207E) provides extra electrostatic interaction with neighboring amino acids which supports the stability of the binding interfaces. Thus the stability of the mutant models observed by computational approach, might help in enhanced acetylation of INH and detoxification, resulting in isoniazid resistance in addition to the over expression of the enzyme when exposed to the drug.

KEYWORDS: NAT; isoniazid; Mycobacterium tuberculosis; mutation; Molecular Dynamics.

INTRODUCTION
Tuberculosis (TB), remains a major cause of public health problems globally. Nearly, 33% of the global population is considered to be infected with *Mycobacterium tuberculosis* (MTB), with 9.6 million new patients and 1.5 million deaths in the year 2014, including 0.4 million deaths among human immunodeficiency virus (HIV)-positive individuals.[1] Besides increasing emergence of multidrug-resistance (MDR), extensively drug-resistant (XDR) TB has also been an increasing risk in some regions around the world.[2,3] Drug resistance in MTB occurs from spontaneous chromosomal mutations at low frequency.[4] Most drug-resistant clinical strains are resistant to isoniazid (INH) and rifampicin (RIF), first-line anti-tuberculous drugs.[5, 6] INH, known as isonicotinyl hydrazine, is an organic compound with simple structure containing two essential components (*i.e.* a pyridine ring and a hydrazide group) required for the high activity against MTB.[7]

The mechanism of resistance of INH has been the subject of extensive study. Sandgren *et al.*(2009) compiled a comprehensive list of the genetic-polymorphisms associated with first and second line drug resistance in clinical MTB isolates throughout the world and reported that there were 22 genes of MTB which were associated with INH resistance.[8] It is widely reported that resistance to isoniazid in MTB has been linked with mutations in genes encoding (i) mycobacterial catalase-peroxidase (katG), the catalase-peroxidase responsible for the conversion of INH into its active form; (ii) InhA protein, (iii) KasA, a β-ketoacyl ACP synthase; (iv) ahpC, an intergenic region responsible for oxidative stress response; and (v) NADH dehydrogenase, encoded by ndh.[9]

Interestingly, like KatG, arylamine N-acetyltransferase (NAT), a drug-metabolizing enzyme, directly interacts with INH and acetylates INH by transferring an acetyl group from acetyl coenzyme A to the terminal nitrogen of the drug, which in its N-acetylated form i.e. N-acetylate INH, is therapeutically inactive.[10] The over

expression of NAT in *Mycobacterium smegmatis* explains increased resistance to INH;[11] in addition, when the gene was knocked-out, the bacteria exhibited increased sensitivity to INH.[12] Therefore, it is likely that NAT competes with KatG for INH (Fig. 1).

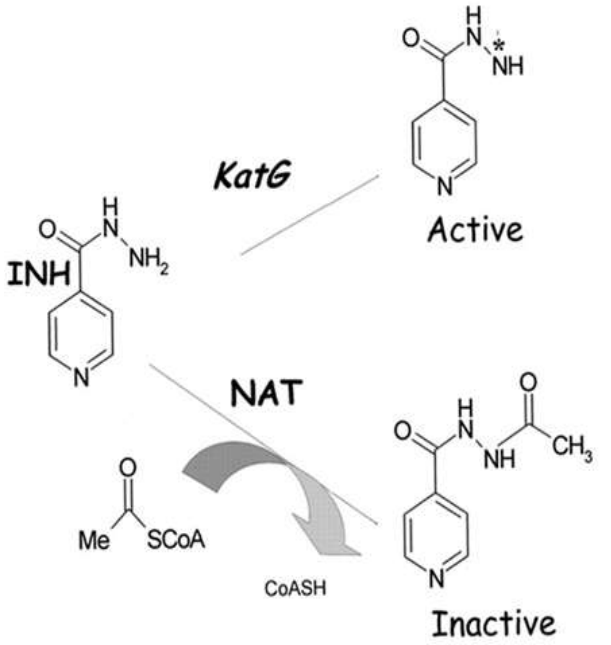

Fig. 1: Schematic representation to show activation and inactivation of INH. INH requires activation by the catalase peroxidase protein (KatG).[10] The NAT enzymes can N-acetylate INH, rendering the drug therapeutically inactive. The asterisk next to the terminal nitrogen in the active form of INH denotes a range of oxidized species.[13]

As INH, is a prodrug and must be activated by oxidation by KatG, which has both catalase and peroxidase activities and the activated drug is thought to exert its effect, at least partially, through inhibition of an enoyl-acyl carrier protein (ACP) reductase (InhA). If isoniazid is acetylated by NAT, the product N-acetylisoniazid cannot be converted to its active form by KatG.[14] Recent studies have suggested that acetylation of INH by the NAT from *Mycobacterium tuberculosis* (TBNAT) may be possible cause of inactivation of the drug thus resulting in resistant strains.[15] Different mutations in the sequence of MTB NAT enzyme such as G68R, L125M, G67R and G207E were identified in clinical isolates associated with INH resistance.[15,16] A computational study on interaction of NAT wild type, G68R and L125M with INH revealed that these mutations can lead to INH resistance.[15] In this study, Bioinformatics techniques were employed to understand the stability and functional ability of other two mutant enzymes (NAT_G67R and NAT_G207E) as compared to wild type enzyme so as to understand mechanism of INH resistance if any. Further, molecular docking and dynamics simulations approaches were employed to observe the interaction behavior of INH with wild type and mutant enzymes of TBNAT.

MATERIALS AND METHODS

Hardware and software

The study was carried out on Dell Workstation with 32 GB RAM and 2 TB hard discs running in linux operating system. Bioinformatics software, such as GROMACS 5.0.4 and online resources were used in this study.

Arylamine N-acetyltransferase (NAT) of Mycobacterium tuberculosis

NAT enzyme is reported to inactivate the anti-tubercular drug isoniazid and is involved in isoniazid metabolism. Mutation in its gene was reported to involve in INH resistance. Protein sequence of NAT (NCBI Accession No. YP_177989) was retrieved from NCBI. The experimentally determined structure of this protein (PDB ID: 4BGF) obtained through the X-ray diffraction experiment was retrieved from the protein data bank (PDB).[17]

Protein structure prediction and validation

As the PDB structure of MTB NAT, has some missing residues, Modeller9v14[18] was used for modeling the three dimensional structure of the protein. Two mutants of NAT (NAT_G67R and NAT_G207E) were also modeled using Modeller9v14. The predicted protein structures were validated and the refined model reliability was assessed through using ProSA-web.[19] and RCSB validation server.[20]

Ligand preparation and protein-ligand docking

The 3D structure of ligand (INH) was retrieved from the PubChem database.[21] Protein (NAT and NAT mutants) - ligand (INH) docking studies were performed using the AutoDock4.2 program[22] as described by Jena *et al.* (2014).[23] All the pre-processing steps for ligand and protein files were performed using the AutoDock Tools 1.5.4 program (ADT) which has been released as an extension suite to the Python Molecular Viewer. The ADT program was used to prepare receptor molecule (NAT) by adding all hydrogen atoms into the carbon atoms of the receptor and Kollman charges were also assigned. For docked ligands, non-polar hydrogens were also added. Gasteiger charges were assigned and torsion degrees of freedom were allocated by the ADT program.

The Lamarckian genetic algorithm (LGA) was applied to model the interaction pattern between receptors and the ligand. The grid maps representing the receptor proteins in the docking process were calculated using Auto Grid (part of the Auto Dock package). A grid of 30, 30 and 30 points in x, y and z directions was centered on the known active site residues (Cys70, His110, Asp127) of each protein. For all docking procedures, 10 independent genetic algorithm (GA) runs with population size 150 were considered for each molecule under study. A maximum number of 25 x 10^5 energy evaluations; 27,000 maximum generations; a gene mutation rate of

0.02 and a crossover rate of 0.8 were used for Lamarckian genetic algorithm. The Auto-Dock program was run in order to prepare corresponding DLGs (docking log files) for further analysis.

Molecular dynamics simulation

The molecular dynamics simulations were carried out for independent NAT wild type protein as well as mutants (G67R and G207E) using GROMACS 5.0.4 package[24] along with GROMOS96 54a7 force field. Initially all models were solvated by simple point charge (SPC) water model embedded in cubic simulation boxes with minimum edge distance of 10 Å. In order to make the systems electrically neutral, one chlorine ion was added by replacing water molecule.[25] Subsequently, all the systems were subjected to a steepest descent energy minimization until reaching a tolerance force of 100 kJ/mol. Further, the systems were equilibrated at 300 K for 100 ps (NVT) by restraining all the protein backbone heavy atoms following by 100 ps of pressure equilibrium (NPT). All the restraints were withdrawn during the NPT equilibration. The velocity rescale thermostat[26] as used for temperature coupling with a time constant (τT) of 0.1 ps for unbound case and 0.8 ps for bound case, isotropic Parrinello-Rahman barostat[27] set to 1.0 bar in all directions with a time constant (τP) of 2.0 ps was considered for pressure coupling. The particle mesh Ewald method[28] was used to treat long-range Coulomb interactions. The All bond lengths were constrained using the linear constraint solver (LINCS) algorithm[29] allowing a time step of 2 fs. Van der Waals force and coulomb interactions cutoff distances were maintained at 1.0 nm. Finally, 100 ns MD simulations of each system were performed.

Again, the docking complexes of isoniazid (INH) with wild type and mutant (G67R and G207E) models of NAT were subjected to MD simulation using the same protocol as described above. Topology of isoniazid (INH) was generated by the PRODRG server.[30] Here, instead of adding single anions, the systems were neutralized electrically by 0.1 mM of NaCl. During the equilibration, protein and ligand were treated as a single group and water with ions as another. The rest procedure was exactly same as described before.

All the important analyses were performed by gromacs analysis programs. Microsoft Excel was used for preparation of the graph.

Visualization

The visualization of structure files was done using PyMol molecular graphics system (www.pymol.org) and the graphical interface of the ADT tool.

RESULTS AND DISCUSSION

Arylamine N-acetyltransferases

The NATs (arylamine N-acetyltransferases) are a family of enzymes initially identified as being responsible for the metabolism of arylamines and arylhydrazines by transfer of an acetyl group from acetyl-CoA to the terminal nitrogen group of the substrate. NAT of MTB has 283 amino acids in its protein sequence. This is an important enzyme of MTB associated with different important pathways of MTB such as nitrotoluene degradation, biosynthesis of secondary metabolites, microbial metabolism in diverse environments etc (http://www.genome.jp/dbget-bin/www_bget?mtu:Rv3566c).

When the nat gene was deleted in *M. smegmatis*[12] and also in *M. bovis* BCG, it was found that the characteristic mycobacterial cell wall lipid components were not present in the NAT deleted strain of *M. bovis* BCG but complementation with nat restored the wild type phenotype. These studies suggested that nat has either a direct or an indirect role in cell wall lipid metabolism and nat gene as essential for survival of *M. bovis* BCG within macrophage. Inhibitors of the other genes in the operon which are essential for survival of *M. tuberculosis* in macrophage have been demonstrated to affect the cell wall lipid composition in a similar fashion to lack of NAT activity.[31] Recently these genes have been suggested to have a role in cholesterol degradation.[32] As cholesterol is essential as a fuel for mycobacteria inside macrophage, NAT has a role in intermediary metabolism and energy production in mycobacteria inside macrophage.[33]

Protein structure prediction and validation

The single amino acid mutation at codon position 67, i.e., Gly to Arg (GGC-GGT) and at 207, i.e., Gly to Glu (GGG-GAG) of nat gene was reported to be associated with INH resistance. Though the three dimensional structure of NAT (PDB ID: 4BGF) is available at PDB, it has some missing residues in its structure file. Thus, the protein model of NAT (Fig. 2a) was generated and subjected for validation along with two mutant models NAT_G67R (Fig. 2b) and NAT_G207E (Fig. 2c).

The stereochemistry of the NAT (wild type) model (Procheck analysis) revealed that 87.9% of residues were situated in the most favorable region and 11.6% were in allowed regions, whereas only one residue (0.4%) fell in disallowed region of the Ramachandran plot (Fig. 2d). The procheck analysis of the mutant NAT model (G67R) revealed that 86.3% of residues were situated in the most favorable region and 12.4% were in additional allowed regions, whereas 0.8% and 0.4% of the residues fell in the generously allowed and disallowed region of the Ramachandran plot (Fig. 2e) respectively. In the case of the NAT (G207E) model, 87.1% of residues were found in the most favorable region and 12.0% in the additional allowed regions and 0.8% of the residues fell in the disallowed region of the Ramachandran plot (Fig. 2f).

ProSA-web evaluation revealed a compatible Z score value of -7.03, -7.36 and -7.33 for the NAT wild type and mutants (G67R and G207E) models respectively, which are well within the range of the native

conformations of crystal structures (Fig. 2 g, h, i). The overall residue energies of both the mutant models were largely negative.

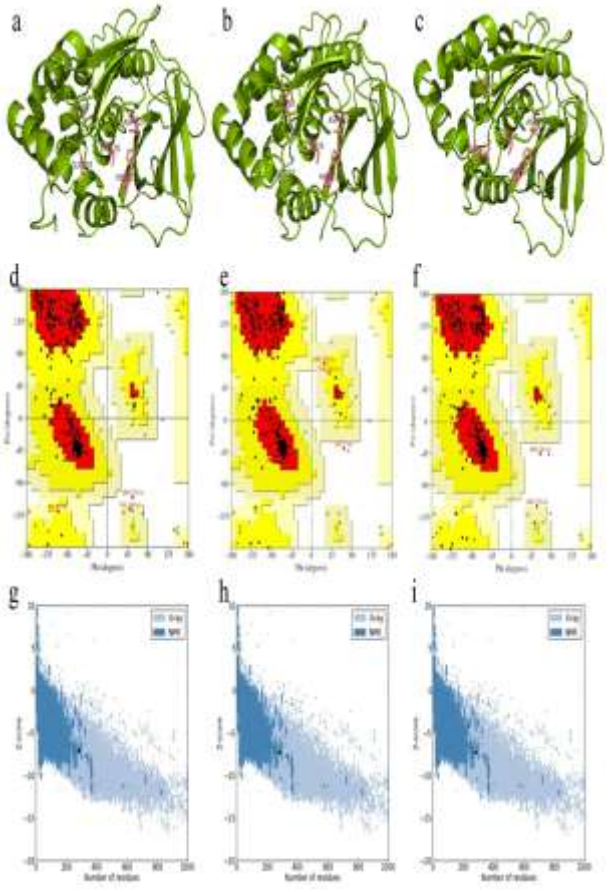

Fig. 2: Protein three dimensional model of (a) NAT (b) NAT_ G67R (c) NAT_ G207E showing important active site residues. Ramachandran plot of (d) NAT wild type model, (e). NAT mutant model (NAT_G67R), (f) NAT mutant model (NAT_G207E). Z plot of (g) NAT wild type, (h) NAT mutant (NAT_G67R). (i) NAT mutant (NAT_G207E).

Docking analysis of NAT (wild type and mutant) and Isoniazid

On the basis of predicted structures of wild type and mutant NAT, the protein ligand (INH) docking was performed using Autodock 4.2 software**.**

From docking analysis, it was observed that INH binds with NAT (wild type) with binding energy of -4.61 kcal/mol and the inhibition constant of the protein–ligand complex was found to be 416.09 µM, whereas in the case of NAT _G67R and NAT_G207E mutants, the binding energy were found to be -4.46 kcal/mol and -4.84 kcal/mol and with inhibition constant of 538.63 µM and 283.16 µM, respectively. As, INH binds with both NAT wild type and mutant proteins with similar binding energy, the protein-ligand complexes were subjected for molecular dynamics simulation analysis to observe the stability of the protein in protein-ligand complex. The protein-ligand interaction before simulation (Fig. 3 a, b, c) and after simulation of 100 ns (Fig. 3 d, e, f) were plotted through LigPlot analysis revealed that the active site residues remains almost similar in all the interaction models.

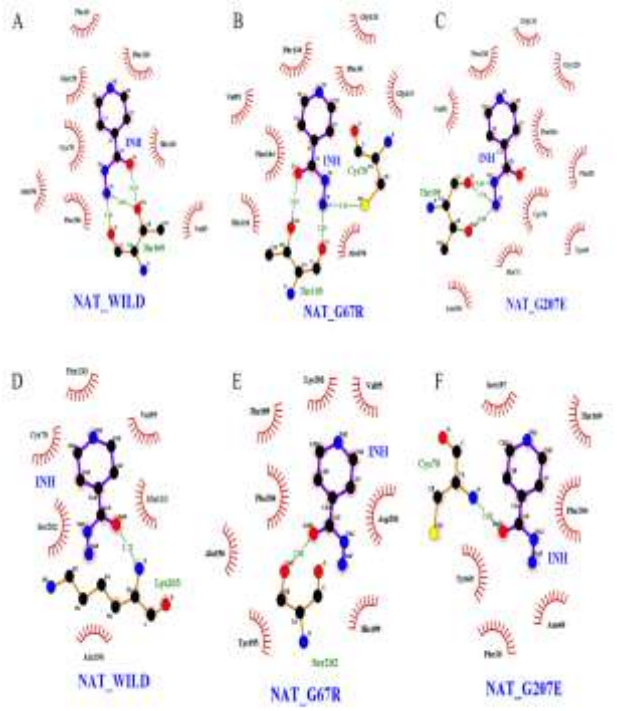

Fig. 3: Docking interaction of INH with (a) NAT_WILD, (b) NAT_G67R, (c) NAT_G207E before simulation and (d) NAT_WILD, (e) NAT_G67R, (f) NAT_G207E after simulation.

Stability of NAT wild type along with its mutant in unbound and bound case

To observe the structural and functional behavior of the wild type as well as mutant protein, molecular dynamics simulation study was performed for NAT wild type and mutant proteins. We performed the RMSD, RMSF and Radius of gyration (Rg) analysis between NAT wild type and mutant (NAT_ G67R and NAT_G207E) protein structures for their stability. In Fig. 4(a), wild type and both mutant structures showed very similar way of deviation till ~18 ns of simulation from their starting structure, resulting in a backbone RMSD of ~0.12 to 0.46 nm. There were not much structural deviation in all the structures till ~54 ns except the NAT_ G207E which was found to be little down as compared to wild type and NAT_G67R. Furthermore after ~54 ns, the wild type structure retained the highest deviation of RMSD of ~0.46 to ~0.57 nm till the end of the simulation. The mutants NAT_G67R and NAT_G207E showed the minimum deviation ranging between ~0.33 to ~0.44 nm and ~0.28 to ~0.41 nm, respectively. The significant variation in the average RMSD values of wild type and mutant structures after the relaxation period (~0.15 nm) may lead to the conclusion that the mutations could increase the protein stability that might enhance the

functional ability of the mutant proteins, thus providing a suitable basis for further analyses. In case of protein-ligand complex, the sudden rise of RMSD plot was observed in the bound state of mutant model NAT_G207E which was caused due to the bend of four anti-parallel beta sheets near C-terminal end (starting at residue 208). These beta sheet complex remains surrounded within the solution in free and don't have any contacts with other segments of protein. In overall, the total RMSD was down in bound state (Fig. 4b) than unbound. In bound case the RMSD was observed around ~ 3 Å for wild type whereas RMSD for NAT_G67R it was around ~ 2-2.5 Å. Further, in case of NAT_G207E, it was above 4 Å and this was again caused due to the bend of that particular beta sheet assembly. But, the secondary structure elements were almost conserved in all models.

For determining the mutation effect on dynamic behavior of residues, the C-α RMSF values of mutant and native structures were calculated. RMSF value of native residues fluctuates within a range between ~0.04 and ~0.49 nm in the entire simulation period without considering few C-terminal amino acids. Moreover mutant model NAT_G67R and NAT_G207E fluctuated within ~0.37 nm and ~0.38 nm respectively, while wild type showed a maximum flexibility of about 0.49 nm (Fig. 4c). The initial large peak in RMSF plot was observed in all the models of NAT and this might be due to the presence of small α helical conformation held by a long loop at the N-terminal part of each model. Further, the other peaks represent the interconnecting loops of beta sheets. Helical contents are relatively more rigid than sheets, found in every model both in bound and unbound states. All the residues were observed to fluctuate in same manner in unbound state of all the models but in case of bound state, the N-terminal region of NAT207 fluctuate more in comparison to others (Fig. 4d). Similarly, the two interconnecting loops of C-terminal sheet of NAT207 were highly excited as the whole beta sheet patch bends away from the protein core. In case of wild type, the interconnecting loops between first and two beta sheet (from N-terminal) was comparatively more excited. The same type of fluctuation was also observed near the C-terminal helical region. By comparing individual amino acid fluctuation in bound and unbound state of each model, we found that, the binding site residues were comparatively more stable in bound case than the unbound. As, most of the binding site residues are present in the secondary structure elements rather than the loops, all the interconnecting loops were fluctuating heavily in bound state of all models than the unbound. The radius of gyration (Rg) is the mass-weighted root mean square distance of group of atoms from their common centre of mass. Hence it provided an observation into global dimension of protein. Radius of gyration graph for alpha-carbon atoms of protein versus time at 300 K was depicted. We observed a major fluctuation in both native and mutants between a time periods of 0 to 100 ns for unbound (Fig. 4e) and bound state (Fig. 4f). Based on Rg plot (Fig. 4e), mutant structures were found more stable than the native.

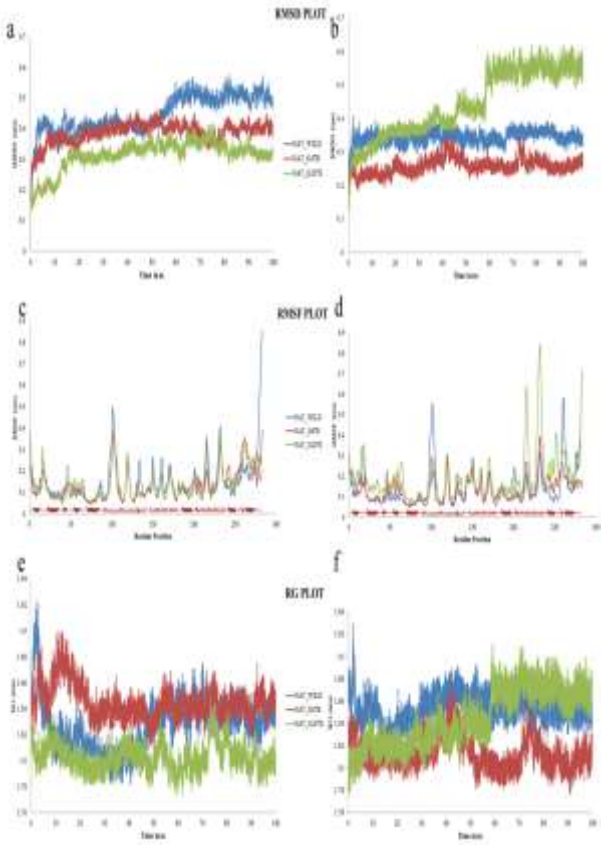

Fig. 4: RMSD plot of NAT models (a) Bound (b) Unbound state. RMSF plot of NAT wild type and mutant proteins (c) Bound (d) Unbound state. Radius of gyration plot of NAT wild type and mutant proteins (e) Bound (f) Unbound state obtained from MD simulation analysis of protein structures.

We have calculated the H-bonds and their percentage of occurrence to the ligand contributed by individual amino acid for each model. It shows that the pattern of H-bonds is very much dissimilar in every model (Fig. 5). By comparing the H-bond pattern with the RMS fluctuations of amino acid in ligand bound state of each model, we found that the amino acid which provide firm H-bond interaction with the ligand, most likely to fluctuate less and the residue that interact in a transient manner have tendency to fluctuate more (Fig. 5).

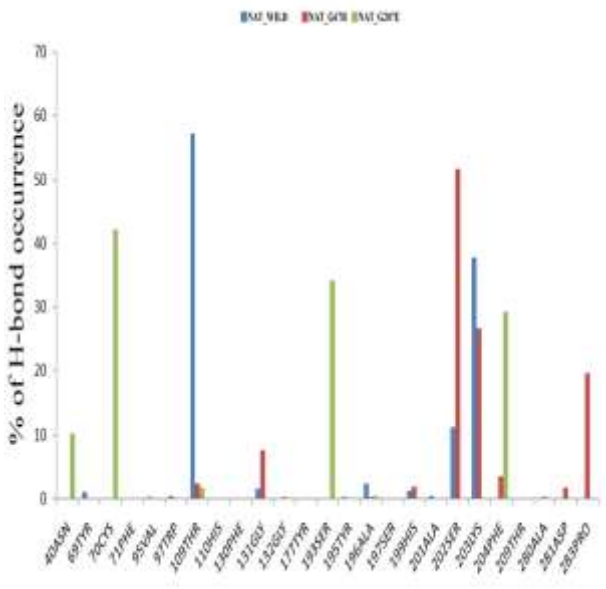

Fig. 5: Pattern H-bond with ligand in all complexes.

Protein-ligand interaction energy analysis

From the protein-ligand interaction energy analysis, it was observed that amino acid residues of all three models interacted differently with INH (Fig. 6). The average interaction energy (sum of coulomb and van-der-walls interaction) of wild type, NAT_G67R and NAT_G207E mutants were found to be -152.5898, -152.9241 & -136.5412 kJ/mol respectively. In comparison to the wild type, NAT_G67R contributed increased polar or electrostatic (coulombic) and decreased nonpolar or van der waals (LJ) interaction, while the NAT_G207E has decreased electrostatic interaction. Further, in order to analyze the interaction energy contribution of individual residues, the residues providing average interaction energy less than -5 kJ/mole were taken into consideration. NAT has four important regions of substrate binding i.e. near Glu39 (Coil region), Cys70 (α-Helix), His110 (β-sheet) and Lys203 (a small α-Helix). In case of wild type the total interaction energy was well distributed by all the above four segments. Thr109 provided the highest interaction energy as coulombic, which was obsolete in two mutant cases. The active site residue Cys70 was observed to be active in wild type and in NAT_G207E, by providing very strong interaction. In NAT_G207E, the first two segments (coil and α-Helix region) were comparatively more attached with the ligand than the other parts. An interesting feature was observed in G67R case, where the C-terminal end folded in such a way that Asp281 and Pro283 provided surprisingly increased interaction. This was not observed in the other two models. Overall, the Van-der-walls interaction ruled over the coulombic in every model.

Further, Gly at position 67 faces Glu39 of the long connector between the fourth and fifth α helix from N-terminal end. Mutation of Gly by a positively charged Arg at this position brings these two amino acids closer by electrostatic interaction and makes the binding site pocket comparatively more stable. Hence, the residues of this mutant model fluctuate less both in bound and unbound case. In case of G207E mutation, the negatively charged amino acid Glu207 interacts with its neighboring Lys203 and forms a pseudo helical conformation in the connecting loop between 7th helix and second beta sheet assemblies, providing extra stability to the binding interfaces.

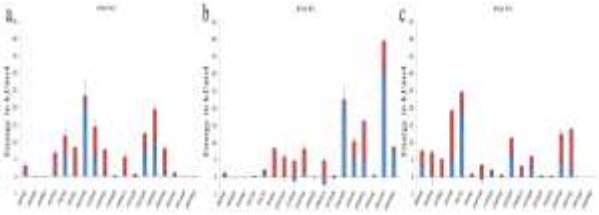

Fig. 6: Protein-ligand interaction energy graph for (a) NAT_WILD, (b) NAT_G67R, c) NAT_G207E showing interaction energy with important active site residues.

Raju *et al* (2015) in their *in silico* simulation studies revealed that there is a surface alteration in dihydrofolate reductase (DHFR) enzyme of MTB due to Glu84Gly (E84G) mutation and further confirmed that due to this mutation there is increased affinity towards its natural substrate dihydrofolate (DHF) and Trimethoprim, a known DHFR inhibitor through *in vitro* study.[34] Ramos *et al* (2012) also employed molecular dynamics simulation approach on other mutants of TB NAT (G68R and L125M) and suggested that these mutations can produce MTB strains resistant to isoniazid.[15] In our MD simulation analysis, we observed that the NAT mutant models were comparatively more stable than the wild type protein independently as well as in protein-ligand complex which might enhance the functional ability of NAT mutants, causing INH resistance.

CONCLUSION

Effect of single amino acid substitution on the stability of the protein remains an important aspect of study in protein science. Different mutations in the form of amino acid substitutions in NAT of MTB were identified in INH resistance strain. To examine the structural consequences of these mutations, MD simulations of unbound protein and protein in complex with INH (wild type and mutant) were performed. It was observed that NAT mutant models (NAT_G67R, NAT_G207E) were comparatively more stable than wild type protein. The enhanced stability of the mutant models might increase the functional ability of the enzyme to perform acetylation of INH as compared to wild type, which leads to formation of inactivated INH that causes drug resistance.

ACKNOWLEDGEMENTS

Authors thank Department of Biotechnology, Ministry of Science & Technology, Government of India for financial support to Bioinformatics Centre wherein this study has been carried out. Authors convey thanks to

Shri Dhiru S Mehta, President, KHS for his keen interest and encouragement.

REFERENCES

1. World Health Organization (2014), WHO Global Tuberculosis Report 2014, World Health Organization, Geneva, Switzerland.
2. Shah NS, Wright A, Bai GH, et al. Worldwide emergence of extensively drug-resistant tuberculosis. Emerg. Infect. Dis, 2007; 13: 380–387.
3. Almeida Da Silva PE, Palomino JC. Molecular basis and mechanisms of drug resistance in Mycobacterium tuberculosis: classical and new drugs. J Antimicrob Chemother, 2011; 66(7): 1417-1430.
4. Zhang Y, Yew WW. Mechanisms of drug resistance in Mycobacterium tuberculosis. Int J Tuberc Lung Dis, 2009; 13(11): 1320-1330.
5. Marrakchi H, Lanéelle G, Quémard A. InhA, a target of the antituberculous drug isoniazid, is involved in a mycobacterial fatty acid elongation system, FAS-II. Microbiology, 2000; 146 289–296.
6. Sarathy JP, Dartois V, Lee EJ. The role of transport mechanisms in mycobacterium tuberculosis drug resistance and tolerance. Pharmaceuticals (Basel), 2012; 5(11): 1210-1235.
7. Middlebrook G, Cohn ML. Some observations on the pathogenicity of isoniazid-resistant variants of tubercle bacilli. Science, 1953; 118(3063): 297-299
8. Sandgren A, Strong M, Muthukrishnan P, Weiner BK, Church GM, Murray MB. Tuberculosis drug resistance mutation database. PLoS Med, 2009; 10; 6(2): e2. doi: 10.1371/journal.pmed.1000002.
9. Hazbon MH, Brimacombe M, Bobadilla del Valle M, Cavatore M, Guerrero MI, Varma-Basil M, Billman-Jacobe H, Lavender C, Fyfe J, García-García L, León CI, Bose M, Chaves F, Murray M, Eisenach KD, Sifuentes-Osornio J, Cave MD, Ponce de León A, Alland D. Population genetics study of isoniazid resistance mutations and evolution of multidrug resistant Mycobacterium tuberculosis. Antimicrob. Agents Chemother, 2006; 50: 2640–2649.
10. Sandy J, Holton S, Fullam E, Sim E, Noble M. Binding of the anti-tubercular drug isoniazid to the arylamine N-acetyltransferase protein from Mycobacterium smegmatis. Protein Sci, 2005; 14(3): 775-782.
11. Payton M, Auty R, Delgoda R, Everett M, Sim E. Cloning and characterization of arylamine N-acetyltransferase genes from Mycobacterium smegmatis and Mycobacterium tuberculosis: increased expression results in isoniazid resistance. J Bacteriol, 1999; 181(4): 1343-1347.
12. Payton M, Gifford C, Schartau P, Hagemeier C, Mushtaq A, Lucas S, Pinter K, Sim E. Evidence towards the role of arylamine N-acetyltransferase in Mycobacterium smegmatis and development of a specific antiserum against the homologous enzyme of Mycobacterium tuberculosis. Microbiology, 2001; 147(Pt 12): 3295-3302.
13. Bodiguel J, Nagy JM, Brown KA, Jamart-Grégoire B. Oxidation of isoniazid by manganese and Mycobacterium tuberculosis catalase-peroxidase yields a new mechanism of activation. J Am Chem Soc, 2001; 123(16): 3832-3833.
14. Sandy J, Mushtaq A, Kawamura A, Sinclair J, Sim E, Noble M. The structure of arylamine N-acetyltransferase from Mycobacterium smegmatis--an enzyme which inactivates the anti-tubercular drug, isoniazid. J Mol Biol, 2002; 3189(4): 1071-1083.
15. Ramos RM, Perez JM, Baptista LA, de Amorim HL. Interaction of wild type, G68R and L125M isoforms of the arylamine-N-acetyltransferase from Mycobacterium tuberculosis with isoniazid: a computational study on a new possible mechanism of resistance. J Mol Model, 2012; 18(9): 4013-4024.
16. Ramaswamy SV, Reich R, Dou SJ, Jasperse L, Pan X, Wanger A, Quitugua T, Graviss EA. Single nucleotide polymorphisms in genes associated with isoniazid resistance in Mycobacterium tuberculosis. Antimicrob Agents Chemother, 2003; 47(4): 1241-1250.
17. Abuhammad A, Lowe ED, McDonough MA, Shaw Stewart PD, Kolek SA, Sim E, Garman EF. Structure of arylamine N-acetyltransferase from Mycobacterium tuberculosis determined by cross-seeding with the homologous protein from M. marinum: triumph over adversity. Acta Crystallogr D Biol Crystallogr, 2013; 69(Pt 8): 1433-1446.
18. Eswar N, Eramian D, Webb B, Shen MY, Sali A. Protein structure modeling with MODELLER. Methods Mol Biol, 2008; 426: 145-159.
19. Wiederstein M, Sippl MJ. ProSA-web: interactive web service for the recognition of errors in three-dimensional structures of proteins. Nucleic Acids Res., 2007; 35: W407-W410.
20. Laskowski RA, MacArthur MW, Moss DS, Thornton JM. PROCHECK: a program to check the stereochemical quality of protein structures. J Appl Crystallogr, 1993; 26: 283-291.
21. Wang Y, Xiao J, Suzek TO, Zhang J, Wang J, Bryant S. PubChem: a public information system for analyzing bioactivities of small molecules. Nucleic Acids Res, 2009; 37: W623–W633.
22. Morris GM, Huey R, Lindstrom W, Sanner MF, Belew RK, Goodsell DS, Olson AJ. AutoDock4 and AutoDockTools4: Automated docking with selective receptor flexibility. J Comput Chem, 2009; 30(16): 2785-2791.
23. Jena L, Waghmare P, Kashikar S, Kumar S, Harinath BC. Computational approach to understanding the mechanism of action of isoniazid, an anti-TB drug. Int J Mycobacteriol, 2014; 3(4): 276-282.
24. Abraham MJ, van der Spoel D, Lindahl E, Hess B and the GROMACS development team (2014)

GROMACS User Manual version 5.0.4, www.gromacs.org.
25. Jorgensen WL, Chandrasekhar J and Jeffry D. Roger W, Impey and Michael L. Comparison of simple potential functions for simulating liquid water. J Chem Phys, 1983; 79: 926.
26. Bussi G, Donadio D, Parrinello M. Canonical sampling through velocity rescaling. J Chem Phys, 2007; 126: 014101.
27. Parrinello M and Rahman A. Polymorphic transitions in single crystals: A new molecular dynamics method. J. Appl. Phys, 1981; 52: 7182-7190.
28. Essmann U, Perera L, Berkowitz ML, Darden T, Lee H and Lee G. A smooth particle mesh Ewald method. J Chem Phys, 1995; 103: 8577.
29. Hess B, Bekker H, Berendsen HJ, Fraaije JG. LINCS: a linear constraint solver for molecular simulations. J Comput Chem, 1997; 18: 1463-1472.
30. Schuttelkopf AW, van Aalten DM. PRODRG: a tool for high-throughput crystallography of protein-ligand complexes. Acta Crystallogr., Sect. D: Biol. Crystallogr, 2004; 60: 1355-1363.
31. Anderton MC, Bhakta S, Besra GS, Jeavons P, Eltis LD, Sim E. Characterization of the putative operon containing arylamine N-acetyltransferase (nat) in Mycobacterium bovis BCG. Mol Microbiol, 2006; 59(1): 181-192.
32. Van der Geize R, Yam K, Heuser T, Wilbrink MH, Hara H, Anderton MC, Sim E, Dijkhuizen L, Davies JE, Mohn WW, Eltis LD. A gene cluster encoding cholesterol catabolism in a soil actinomycete provides insight into Mycobacterium tuberculosis survival in macrophages. Proc Natl Acad Sci U S A, 2007; 104(6): 1947-1952.
33. Pandey AK, Sassetti CM. Mycobacterial persistence requires the utilization of host cholesterol. Proc Natl Acad Sci U S A, 2008; 105(26): 4376-4380.
34. Raju A, Kulkarni S, Ray MK, Rajan MGR, Degani MS. E84G mutation in dihydrofolate reductase from drug resistant strains of Mycobacterium tuberculosis (Mumbai, India) leads to increased interaction with Trimethoprim. Int J Mycobacterio, 2015; 4: 97-103.